SMALL GAS TURBINE GTM-120 BENCH TESTING WITH EMISSION MEASUREMENTS

Maciej Chmielewski, Marian Gieras

Warsaw University of Technology, Institute of Heat Engineering
Nowowiejska Street 21/25, 00-665 Warsaw, Poland
tel.:+48 22 234 52 22
e-mail: marian.gieras@itc.pw.edu.pl

Abstract

The aim of this paper is to provide comprehensive bench testing results for small gas turbine engine with a strong focus on the flue gas emission measurements. After a short overview of small gas turbine GTM-120 design and working principles, the test bench developed at the Institute of Heat Engineering at the Warsaw University of Technology is presented. Capability and accuracy of the sensors used in test bench are discussed in detail. Data acquisition software based on LabVIEW is also presented.

Five separate sections representing successive engine stations have been distinguished. Experimental set of data of pressure and temperature on all of the stations is presented for the whole range of engine rotational speeds. Additionally, the engine thrust and fuel consumption data is provided. Special attention is given to the engine NO_x and CO content in the engine exhaust gas, since turbine engine emissions are of great concern due to their adverse impact on natural environment. Experimental results are followed by the engine cycle parametric study for real engine thermodynamic cycle.

Finally, future work plans regarding variable combustor chamber utilization for emission reduction from small gas turbine are discussed.

Keywords: small gas turbine, emission measurements, combustion engines, bench testing, engine performance

1. Introduction

Miniature gas turbines are becoming widely used in many technical applications such as unmanned aerial vehicles propulsion systems, power and heat generators, even in hybrid electric vehicles. The devices of this kind perfectly fit the current trends of minimization. Historically, miniature gas turbines were amateur constructions used in hobbyist applications. Currently however, restrictive emission standards and economic considerations call for reduction in fuel consumption and emission of pollutants, such as NO_x and CO, in widely available engine applications.

Numbers of publications state a strong demand for miniature gas turbines working parameters and emissions experimental data [2, 4, 11]. Recently an article [7] regarding GTM-120 exhaust gases emissions has been published; however, data presented in the paper are very contentious.

The aim of this article is to present comprehensive, experimental data of small gas turbine working parameters. Data for pressure and temperature for each of the engine flow path stations along with engine thrust and flue gas emissions are presented.

2. Engine and test bench

The object of the study presented in this article is GTM-120 small gas turbine. The engine is single-spool, turbojet engine. Fig. 1 shows main engine components: centrifugal compressor, diffuser, annular combustion chamber with pre-vaporising tubes, turbine nozzle, turbine wheel and nozzle cone. Station identification presented in Fig. 1 is consistent with [9]. The basic engine dimensions are included in Tab. 1. The engine is powered by both gaseous and liquid fuels. Engine start-up is performed with the use of propane, which is fuel that is more reliable during cold start-up conditions. After reaching stable start-up conditions, engine control unit (ECU)

automatically switches fuel system to liquid fuel. Liquid fuel used in the engine is a blend of kerosene (PKN Orlen Jet A-1) with 5% jet engine oil addition (Mobil Jet Oil II) for bearings lubrication and cooling. Approximately 2.5% of fuel-oil mixture is supplied to the bearing space, and it does not take part in the combustion. Engine rotational speed range is ~40k-120k rpm.

Test bench (Fig. 2) consists of GTM-120 small jet turbine with ECU mounted on engine mount, fuel tank, exhaust gas analyser, data acquisition card and PC with test bench software. Pressure and temperature sensors have been placed in 5 engine sections (Fig.1):

- Section 2':
  - Differential pressure sensor: Honeywell ASDX030D44R,
  - Pressure sensor: Kobold SEN-8701/2 B045,
  - Thermocouple Czaki TP-202 (type K),
- Section 3':
  - Two pressure sensors: Kobold SEN-8701/2 B055,
  - Thermocouple: Czaki TP-202 (type K),
- Section 4':
  - Pressure sensor: Kobold SEN-8701/2 B055,
  - Two thermocouples Czaki TP-203 (type K),
- Section 5':
  - Pressure sensor with cooling system: Dudek P400F,
  - Two thermocouples Czaki TP-203 (type K),
  - Gas analyser probe,
- Section 9':
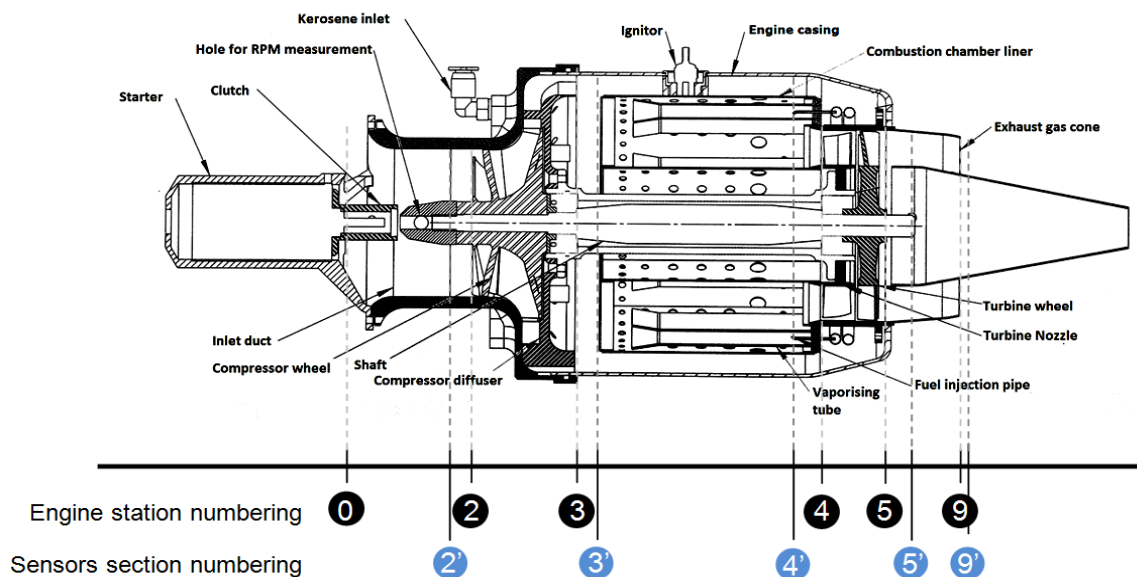 - Two thermocouples Czaki TP-203 (type K).

Fig. 1. Engine cross-section with station numbering

Inlet air mass flow is measured with differential pressure sensor mounted in section 2'. Engine inlet is equipped with two measuring tubes used to measure static and dynamic pressures. Appropriate placement of the tubes was achieved with the use of CFD tools [10].

Engine is mounted on test bench equipped with strain gauge Mavin NS-6 with WOBit WDT-1 strain gauge amplifier used to measure thrust force. Fuel tank is equipped with differential pressure sensor Dudek P400U used to measure fuel consumption. All sensors are connected to the National Instruments USB-6259 BNC card connected to PC with test bench software programmed in LabVIEW 2011.

Tab. 1. Basic engine dimensions

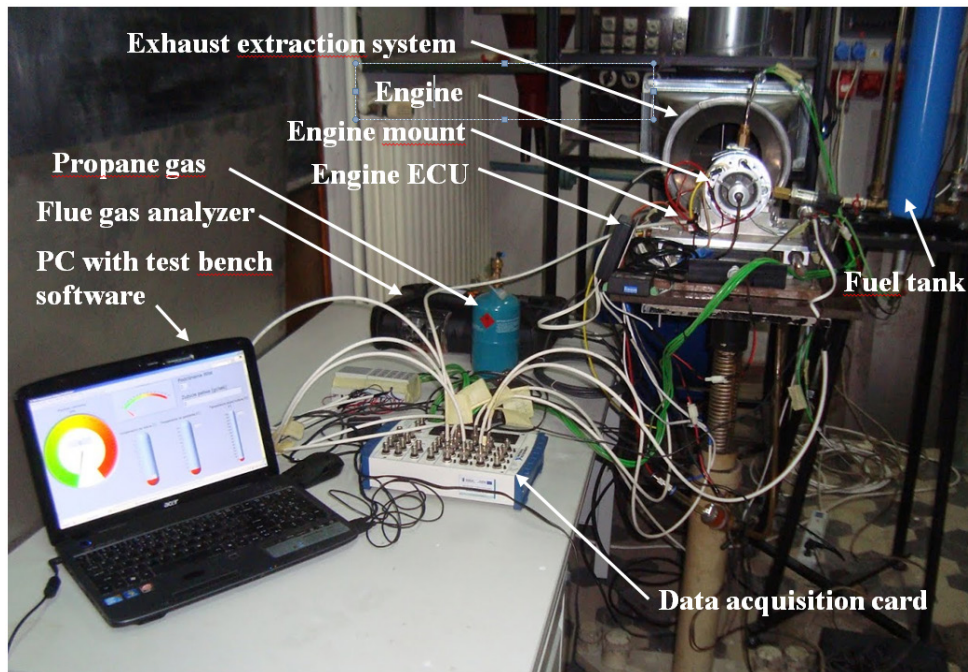| Parameter	Value	Units
Engine mass	1.5	kg
Compressor inlet diameter	54.15	mm
Compressor outlet diameter	70	mm
Turbine wheel diameter	70	mm
Maximum engine diameter	110	mm
Total length	265	mm

Fig. 2. GTM-120 test bench developed at Institute of Heat Engineering, Warsaw University of Technology

Portable emission analyser Testo 350 is used to measure engine exhaust gas composition. Gas analyser was calibrated by manufacturer prior to experimental trials. Custom-made emission probe is located in the engine exhaust cone (section 5') in order to avoid mixing of the exhaust gas with clean air.

3. Experimental results

Total numbers of six experimental trials in the entire range of engine rotational speeds have been performed. All working parameters were registered during each experimental run. For each trial thermocouples at section, 4' were immersed in the combustion chamber at different depths in order to capture temperature profile (radial temperature distribution) of the flow at the combustor outlet. Similarly, thermocouples at section 5' were operating on different radial position in the outlet stream to capture temperature profile. Ambient temperature during the experiments was in the range of +17°C to +19°C, at atmospheric pressure in the range of 1005 hPa to 1016 hPa and relative humidity in the range of 41% to 56%. A single engine trial lasted from 2.5 to 5 minutes. The aim of each experimental run was to capture five stable engine-operating points: 40k, 60k, 80k, 100k and 120k rpm. During each trial engine rotational speed was increased in increments of 20k rpm to reach 120k rpm and then the speed was reduced stepwise (also by 20k rpm). Engine rotational speed was maintained stable for approximately 15 second at each operating point in order to eliminate transient effects. The engine was cooled down to ambient temperature between trials in order to reflect full engine thermal cycle at each run. This also helped to capture hysteresis of engine work parameters. Each trial generated about 7,500

-15,000 data points. Additionally, 30 to 60 data points of O_2, NO, NO_2 and CO emission measurements were obtained during each experiment. Emission analyser probe was set at different radial distances from engine centreline to capture dependency of the probe position on the results. The course of the thrust measurement during selected experimental run is presented in Fig. 3.
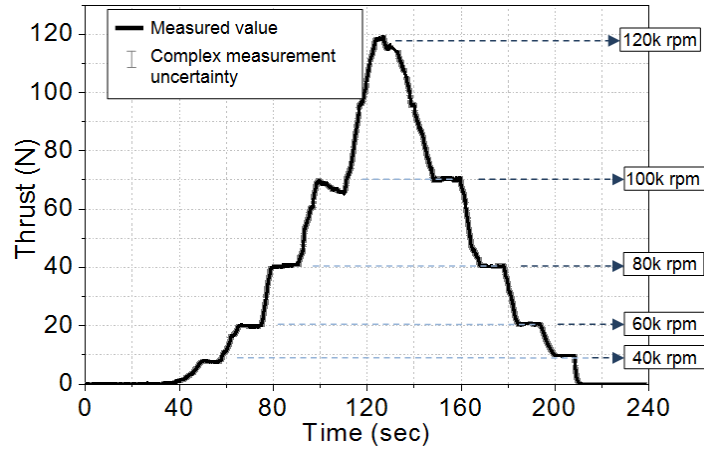

Fig. 3. Course of the trust measurement during one of the experimental runs

A complete experimental uncertainty analysis for each of engine test rotational speeds was carried out. The test results presented in Fig. 4 and 5 are the averaged mean values of the operating parameters at fixed speed. Deviations are treated as the root of the sum of squares of measurement uncertainty and standard deviation of investigated parameter for each test speed.
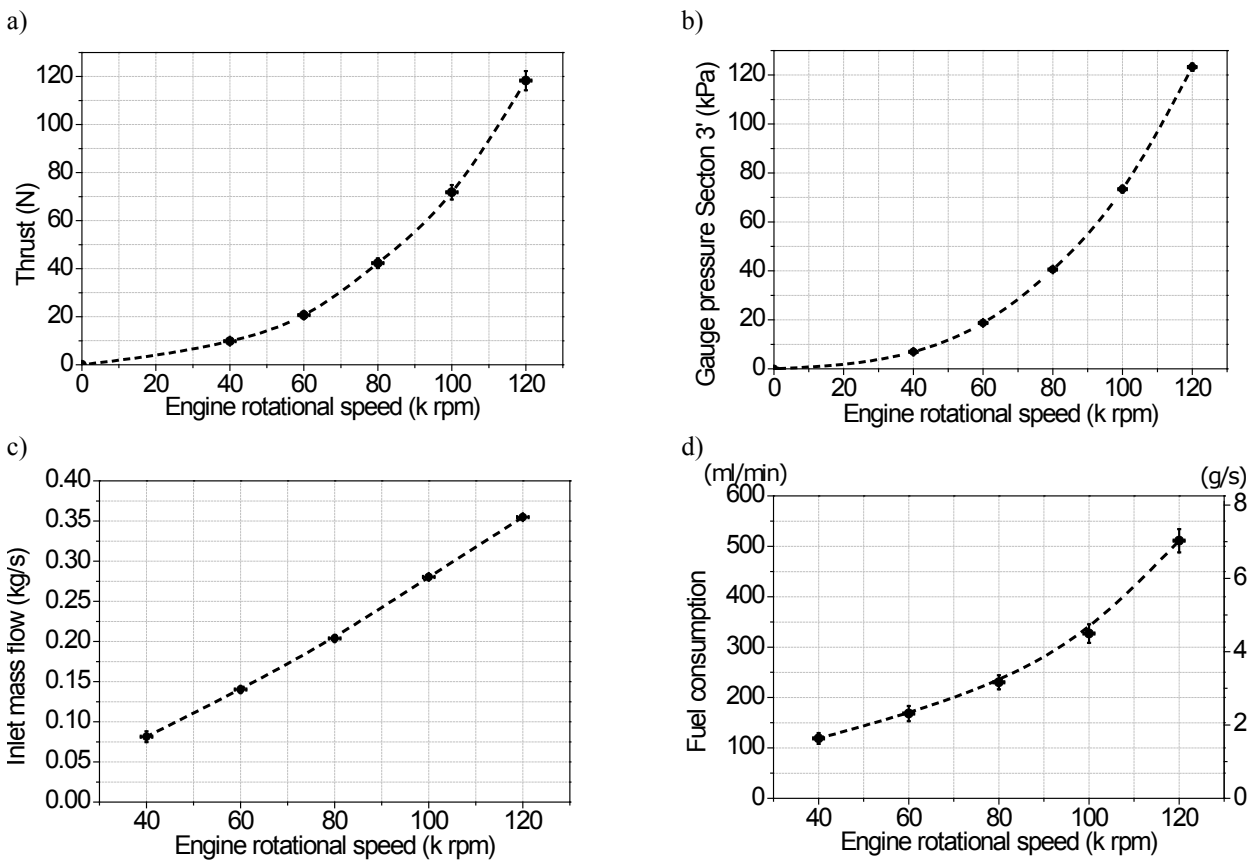

Fig. 4.   Experimental results: a) Thrust; b) Static gauge pressure at compressor outlet (Section 3'); c) Inlet mass flow; d) Fuel consumption
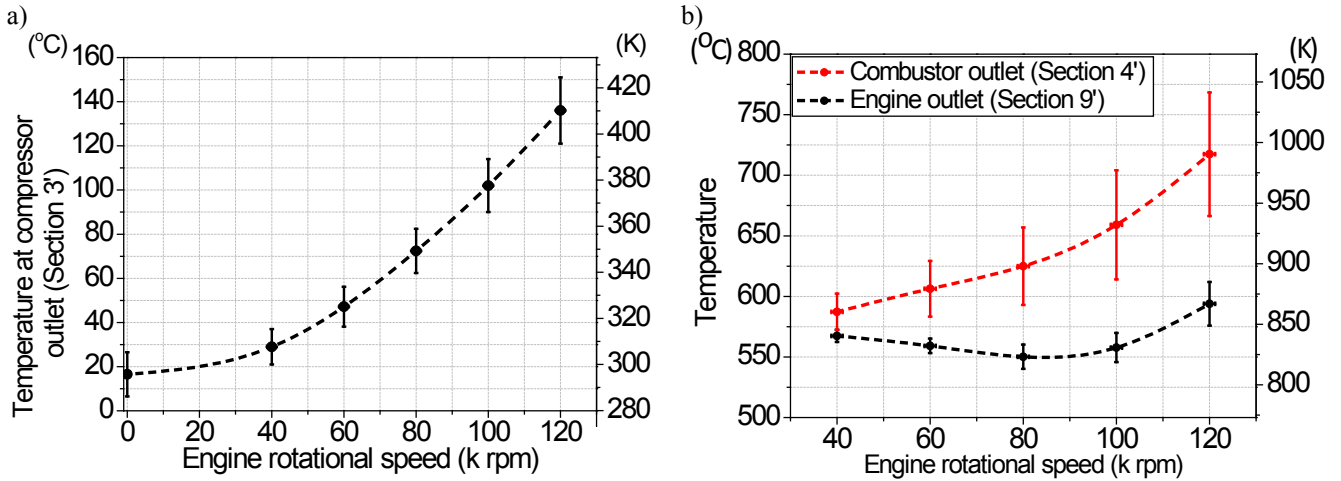
Fig. 5. Experimental results: a) Total temperature at compressor outlet (section 3'); b) Total temperature at combustion chamber outlet (section 4') and nozzle outlet (section 9')
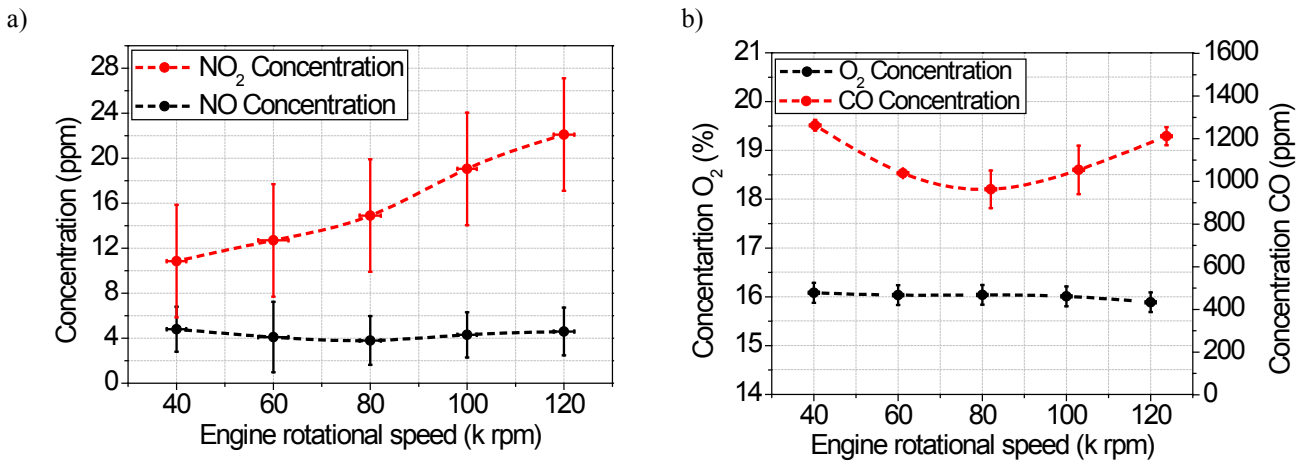

Fig. 6. Experimental results: a) NO and NO₂ concentrations; b) O₂ and CO concentrations

4. Engine cycle efficiency

Based on experimental result presented in Fig. 5 it is possible to calculate real engine thermodynamic cycle efficiency. The real engine thermodynamic cycle for the single shaft jet engine is shown in Fig. 7.
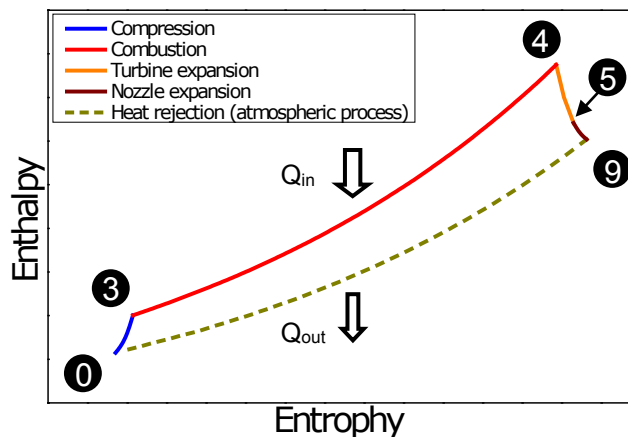

Fig. 7. Real Brayton thermodynamic cycle

In Fig. 7, Q_{in} represents heat added to the cycle in the form of fuel and Q_{out} is heat removed to atmosphere. Of course, Q_{out} refers to a heat loss in the cycle; therefore, the thermodynamic efficiency of the cycle can be described using equation (1).

$$\eta_{th} = \frac{W_{net}}{Q_{in}} = \frac{Q_{in} - Q_{out}}{Q_{in}} = 1 - \frac{(1 + FAR)c_{ph}(T_9 - T_0)}{(1 + FAR)c_{ph}T_4 - c_{pc}T_3}, \qquad (1)$$

where:

W_{net} – cycle network (represented graphically by the internal area bounded by curves in Fig. 7),
FAR – fuel-air mass ratio,
c_{pc} – specific heat of air (=1.4),
c_{ph} – specific heat of exhaust gasses (=1.33),
T_0 – ambient air temperature,
T_3 – air temperature at compressor outlet,
T_4 – exhaust gases temperature at combustor outlet,
T_9 – exhaust gases temperature at nozzle outlet.

In further consideration, it is assumed that temperatures T_3, T_4 and T_9 are equal to measured temperatures $T_{3'}$, $T_{4'}$ and $T_{9'}$.

With the use of above approximations, one can express equation (1) by the formula (2).

$$\eta_{th} = 1 - \frac{(1 + FAR)c_{ph}(T_{9'} - T_0)}{(1 + FAR)c_{ph}T_{4'} - c_{pc}T_{3'}}. \qquad (2)$$

Thermodynamic efficiency calculated with the use of formula (2) is presented in Fig. 8. Accuracy of the efficiency determination is calculated as complex accuracy applying formula (3).

$$\varepsilon_{\eta_{th}} = \sqrt{\sum_i \left(\frac{\partial \eta_{th}}{\partial T_i} \varepsilon_{T_i} \right)^2} \quad \text{for } i \in \{0; 3'; 4'; 9'\}, \qquad (3)$$

where:

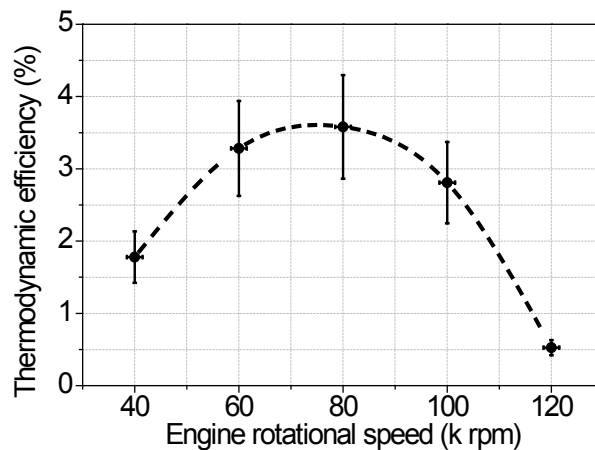ε_{T_i} – accuracy of ith temperature measurement.

Fig. 8. Calculated GTM-120 engine cycle efficiency

5. Comments on results and conclusions

Pressure and temperature results for Section 3' included in Fig. 4 and 5 are consistent with results presented in available literature [5, 8]. However, there is a large variation of temperature at

Section 4'. This variation can be explained by strongly non-uniform temperature profile and pattern (circumferential temperature distribution). Significant reduction in radial and hoop temperature variation at Section 5' occurs because of vigorous exhaust gas mixing in turbine rotor. Therefore, calculated results regarding cycle efficiency presented in Fig. 8 should be treated more as qualitative rather than quantitative.

It is worth noticing that experimental results of NO and NO_2 emissions presented in Fig. 6a are the emissions measured by the emission analyser. The flue gases are transported from probe to the analyser with the use of 1.5 m long hose. Additionally, the analyser has a built-in radiator to cool down the exhaust gases to the temperatures acceptable by the electrochemical measuring cells installed in the analyser. Therefore, the NO/NO_2 ratio reported by the analyser is different than ratio at engine outlet. The reason for that is the rapid oxidation of NO to NO_2 in lower temperatures, the so called "quenching effect". The "quenching effect" is described by the Glarborg-Hadvig mechanism [3]. Impact of NO_x reburning on the exhaust gases composition was described in [1, 12].

The course of NO_x ($NO+NO_2$) presented in Fig. 6a and CO presented in Fig. 6b clearly shows that there is an optimal engine operation point for low emissions. The combustion chamber is the engine component most influencing temperatures in the primary zone, hence CO and NO_x emissions (Fig. 9). Further investigation shows that the low emission point is consistent with the highest engine efficiency point. The conclusion from above is that the geometry of the GTM-120 combustion chamber is optimal for around 80k rpm of rotational speed.
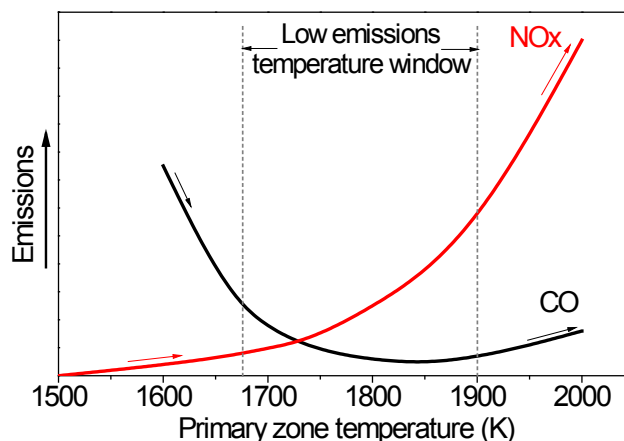

Fig. 9. Influence of primary-zone temperature on CO and NO_x emissions. Based on [6]

Modern large commercial turbojet engines are equipped with the devices aimed to improve engine components' efficiencies over the wide range of rotational speeds. Devices such as VBV (Variable Bleed Valves), VSV (Variable Stator Vane), ACC (Active Clearance Control) are used for adjusting the geometry of the engine for optimum performance. Concept of engine components with variable geometry is essential for continued trend of efficiency increase and NO_x/CO emissions reduction. Utilization of the combustion chamber with variable geometry seems to be a very promising idea, especially in small-scale jet engines as presented in this article.

Future work

Authors are finishing the full annular Computational Fluids Dynamic (CFD) model for the Diffuser-Combustor-Turbine Nozzle engine module for selected steady state engine operating conditions. CFD results are going to be verified against experimental results presented in this paper. Verified numerical settings are going to be used in CFD simulation of combustion inside variable geometry combustor. Authors aim to show both numerically and experimentally advantage of variable geometry combustion chamber concept in terms of efficiency increase and emission reduction over wide range of rotational speeds from small gas turbine engine.

Acknowledgments

References

[1] Braun-Unkhoff, M., Frank, P., Stapf, D., Leuckel, W., *Analysis of NOx Reburning under Plug-Flow Reactor Conditions,* 4th European Conference Industrial Furnaces and Boilers, Portugal 1997.

[2] Gieras, M., Stańkowski, T., *Computational study of an aerodynamic flow through a micro-turbine engine combustor*, Journal of Power Technologies 92 (2), pp. 68-79, Warsaw 2012.

[3] Glarborg, P., Hadvig, S., *Development and Test of a kinetic Model for Natural Gas Combustion*, Nordic Gas Technology Centre, DK 1991.

[4] Gonzlaes, C. A., Wong, K. C., Armfield, S., *Computational study of a micro-turbine engine combustor using large eddy simulation and Reynolds averaged turbulence models*, ANZIAM Journal, Vol. 49, C407-C422, Australia 2007.

[5] Kamps, T., *Model Jet Engines*, Traplet Publications Ltd., UK 2005.

[6] Lefebvre, A. H., Ballal, D. R., *Gas Turbine Combustion: Alternative Fuels and Emissions,* CRC Press, Boca Raton 2010.

[7] Merkisz, J., Markowski, J., Galant, M., Karpiński, D., Kubiak, K., *Badania wpływu dodatku tlenowego (CH3(OCH2CH2)3OCH3) na emisję gazowych składników spalin silnika turbinowego GTM-120*, Oficyna Wydawnicza Politechniki Warszawskiej, Prace Naukowe Politechniki Warszawskiej. Transport, Z. 101, Warsaw 2014.

[8] Schreckling, K., *Home built model turbines*, UK 2005.

[9] Society of Automotive Engineers, *Gas Turbine Engine Performance Station Identification and Nomenclature*, Aerospace Recommended Practice, ARP 755A, Warrandale 1974.

[10] Ślesik, D., *Obliczenia numeryczne dyfuzora małego silnika odrzutowego GTM-120*, Praca dyplomowa magisterska, Warsaw 2013.

[11] Trebunskikh, T. V., Ivanov, A. V., Dumnov, G. E., *FloEFD simulation of micro-turbine engine,* Proceedings of Applied Aerodynamics Conference on Modelling & Simulation in the Aerodynamic Design Process 2012: Current Practice & Future Prospects, Bristol 2012.

[12] Zhuang, J., Leuckel, W., *Formation of Nitrogen Dioxide in Combustion Processes*, Proceedings of the 1998 International Gas Research Conference, IPP-24, pp. 349-360, San Diego 1988.